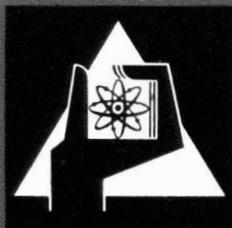# KERNFORSCHUNGSZENTRUM

KARLSRUHE

Juni 1963 KFK 166

Institut für Neutronenphysik und Reaktortechnik

Pulsed Neutron Experiments on Subcritical Heavy
Water Natural Uranium Lattices

H. Meister

PULSED NEUTRON EXPERIMENTS ON SUBCRITICAL HEAVY WATER NATURAL URANIUM LATTICES

H. MEISTER

Institut für Neutronenphysik und Reaktortechnik, Kernforschungszentrum Karlsruhe, Germany

Abstract—Prompt neutron decay in several subcritical D$_2$O-moderated natural uranium lattices has been investigated by the pulsed technique. Employing various detector positions inside the multiplying medium we achieved a separation of flux harmonics by means of a Fourier transform. From the modal decay curves we obtained the prompt neutron decay constant α as a function of geometrical buckling B^2. In the lower buckling region, $B^2 < 25$ m^{-2}, experimental α vs. B^2 curves agree very well with simple two-group calculations on the basis of lattice parameters determined in previous exponential experiments (MEISTER, 1961). Deviations for higher B^2 are shown to be due to spectrum shifts towards lower neutron energies.

In addition, we determined the change of radial buckling $\Delta\mu^2$ due to cadmium rods fully inserted into the lattice. The results are in agreement with stationary experiments as well as two-group calculations. With single fuel rods withdrawn from the lattice, however, the corresponding radial buckling change $\Delta\mu^2$ turns out to be strongly dependent on the buckling of the axial flux distribution.

1. INTRODUCTION

LET us first consider the general time behaviour of the thermal neutron flux $\phi(t)$ after a burst of fast neutrons has been injected into a subcritical reactor system. It may be described in the following way:

(1) During the slowing down period the thermal neutron population is established which may be regarded as a superposition of flux modes characteristic of the geometry of the system.

(2) The various modes die out with decay constants α_k determined by prompt fission neutron balance.

(3) After that, there remains a slowly decaying part of neutrons due to delayed neutron precursors.

Accordingly, the thermal neutron flux $\phi(\mathbf{r}, t)$ in an unreflected system is written as an expansion of eigenfunctions $\varphi_k(\mathbf{r})$

$$\phi(\mathbf{r},t) = \sum_k A_k\varphi_k(\mathbf{r})\{e^{-\alpha_k t} + c_k e^{-\alpha_k'' t}\}, \qquad (1.1)$$

if only one effective group of delayed neutrons is assumed and the slowing down period, which occurs within some 10^{-5} sec in a heavy water moderator, is disregarded. For the fundamental mode the decay constants α and α'' of the prompt and the delayed neutron part, respectively, may be derived from the kinetic equations (GLASSTONE and EDLUND, 1957) as follows

$$\alpha = \frac{1 - k_{\text{eff}}(1 - \beta)}{l_{\text{eff}}} + \frac{\bar{\lambda}\beta k_{\text{eff}}}{1 - k_{\text{eff}}(1 - \beta)}$$

$$= \frac{\rho + \beta}{(\rho + 1)l_{\text{eff}}} + \bar{\lambda}\frac{\beta}{\rho + \beta} \qquad (1.2)$$

$$\alpha'' = \bar{\lambda}\frac{1 - k_{\text{eff}}}{1 - k_{\text{eff}}(1 - \beta)} = \bar{\lambda}\frac{\rho}{\rho + \beta} \quad (\bar{\lambda}l_{\text{eff}} \ll 1) \quad (1.3)$$

where l_{eff} is the effective neutron lifetime and $k_{\text{eff}}(1 - \beta)$ the effective prompt neutron multiplication factor. $\rho = (1 - k_{\text{eff}})/k_{\text{eff}}$ is the negative reactivity, β the delayed neutron fraction and $\bar{\lambda} = \sum_i \beta_i\lambda_i/\sum_i \beta_i = 0.407$ sec^{-1} the average decay constant of the delayed neutron precursors.

In a heavy water moderated system l_{eff} is about 10^{-3} sec. Hence, the condition $\bar{\lambda}l_{\text{eff}} \ll 1$ is fulfilled and the correction term $\bar{\lambda}\beta/(\rho + \beta)$ in equation (1.2) is negligible except for a system close to critical. In a system far from critical, $\rho \gg \beta$, we have in addition $\alpha'' \gg \alpha$ and the delayed neutron part decays very slowly compared with the prompt neutron part.

Present pulsed experiments are mainly based on the exploration of the prompt neutron decay constant α. In principle, there are two types of experiments under consideration:

(a) If the neutron lifetime l_{eff} as well as β are known, the reactivity ρ of a subcritical reactor system may be determined by means of equation (1.2). Furthermore, by measuring α at delayed critical β/l_{eff} can be obtained. This method has often been employed for calibration of control rods and other neutron absorbers, especially for various D$_2$O-moderated reactors (SJÖSTRAND, 1956; SIMMONS and KING, 1958; SILVER et al., 1960; KÜCHLE, 1961).

(b) Pulsed experiments on reactor systems of well-defined geometric shape can be made in order to obtain α as a function of geometrical buckling B^2. Afterwards, experimental results may be compared with $\alpha(B^2)$ calculated on the basis of a theoretical model. In this way, the pulsed method can be used to check reactor theory concepts.

Experiments of this type have been carried out on graphite and light water moderated systems (BENGSTON et al., 1958; CAMPBELL and STELSON, 1956; FULTZ, 1959), but no systematic studies on D_2O systems are available so far. In the present paper, $\alpha(B^2)$ of various D_2O lattices was measured far below critical in the buckling range $13\ m^{-2} < B^2 < 40\ m^{-2}$ for comparison with homogeneous two-group theory.

2. EXPERIMENTAL FACILITIES

The subcritical assembly previously used for ordinary exponential experiments has been extensively described elsewhere (MEISTER, 1961). For the present purpose of pulsed experiments the graphite pedestal containing the Ra-Be source was removed and a d-t accelerator was installed.

2.1 Experimental tank

The experimental tank of $1\cdot36\ m$ dia. and $2\cdot95\ m$ height is suspended from a steel framework. The outer surface of the 5 mm aluminium tank walls is clad with boral sheet of 8 mm thickness in order to provide a well-defined slow neutron boundary condition. The uranium rods are suspended from a system of movable steel beams by means of which the lattice pitch can easily be varied in units of $0\cdot6$ cm.

For having the possibility of D_2O-level adjustment we make use of a storage tank system from which the heavy water can be pumped up into the experimental tank; D_2O-level accuracy is within ± 1 mm.

2.2 Pulsed neutron source

We used a 150 kV Cockcroft-Walton d-t accelerator as a pulsed neutron source (EYRICH, 1962). In order to release a neutron burst, a reference signal given by the time analyser is transmitted to the accelerator by

means of a light pipe system which triggers a square wave generator connected to the extraction electrode of the r.f. ion-source. The pulse length could easily be varied and was 100 μsec in most of our experiments. The ion current on the target was about 3 mA during the pulse, the source background between two pulses being less than 10^{-6} of full intensity.

By means of a 2m-long target tube the tritium target was placed on the central axis below the bottom of the experimental tank. By adjusting the position of the target we could provide for a low excitation of higher radial flux modes.

2.3 Neutron detecting equipment

The neutron detector employed for measuring the thermal flux decay was a small BF_3-counter ($1\cdot3$ cm dia. 5 cm active length) guided by a thin aluminium tube ($1\cdot8$ cm o.d.), which was mounted inside the moderator on the axis of the tank. The preamplifier was placed 3 m from the detector outside the lattice zone in order to avoid flux distortions. An additional BF_3-counter mounted on an eccentric lattice position was used as a monitor for normalizing neutron intensity in successive experiments.

The block diagram of the electronic equipment is shown in Fig. 1. The signal given by a time mark generator starts the timing cycle of the analyser, TMC Model CN-110 with pulsed neutron plug-in unit. First of all, the neutron background is measured within a time interval $b\Delta t$ by a particular background channel. After this, a reference pulse is given to the accelerator to produce a neutron burst and, after a waiting time ($\approx 2\Delta t$), the time-dependence of neutron flux is recorded with a channel width Δt, while there is an insensitive switching time of 10 μsec between each two consecutive channels. In most experiments, we used 128 channels with $\Delta t = 320$ or 640 μsec and a
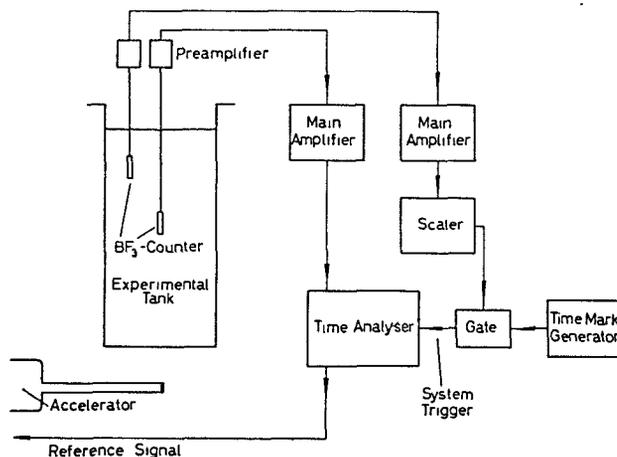

FIG. 1.—Block diagram.

background time ratio $b = 128$. The repetition rate was chosen sufficiently low (10 per sec) so as to permit complete decay of prompt neutrons before starting the background measurement. Hence, the background was merely due to delayed neutrons and spontaneous fission neutrons.

By comparing the flux decay measured at different source intensities, the overall dead time of the equipment was determined to be 1·8 μsec. During actual experiments, dead time corrections were less than 3 per cent.

3. EXPERIMENTS ON UNDISTURBED LATTICES

3.1 Lattice assemblies

Altogether, we investigated four different square lattices (lattice pitch $d = 15\cdot6$ to 21·6 cm) composed of natural uranium metal rods of 3·2 cm diameter, density $\rho = 18\cdot85$ g/cm^3. Figure 2 shows the cross section
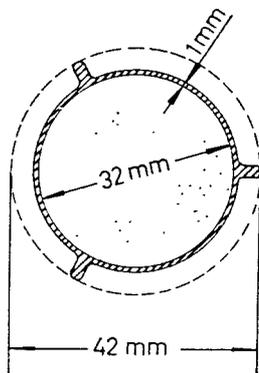
FIG. 2.—Cross section of a fuel rod.

of a fuel rod which is to be used in the Karlsruhe research reactor FR 2. The 1 mm aluminium can is provided with fins for centering the rod inside the flow tube, which was removed, however, in our experiments. The moderator purity was 99·78 mol per cent D$_2$O; heavy water temperature was within 21·0 $\pm$ 1·2°C.

TABLE 1.—LATTICE ASSEMBLIES
(d = lattice pitch, n = number of fuel rods.)

d (cm)	V_M/V_U	n	Number of fuel rods per row of a quadrant
15·6	29·09	52	4 + 4 + 3 + 2
16·8	33·93	52	4 + 4 + 3 + 2
18·0	39·12	44	4 + 3 + 3 + 1
21·6	56·85	32	3 + 3 + 2

The lattice assemblies listed in Table 1 were arranged in such a manner that the neutron counter on the central axis was symmetrically surrounded by four

fuel rods. Because the lower 5 cm of the fuel rods were entirely made of aluminium and the bottom of the experimental tank was slightly vaulted to the inside, we had a reflector zone below the core region. In order to obtain a plain external boundary of the reflector, the volume below the vaulting up to 8 cm high was filled with graphite, the diffusion properties of which are not very different from D$_2$O. By this procedure, we had a bottom reflector of 22 cm effective thickness mainly consisting of heavy water. The influence of this reflector on the experiments is shown to be very small and will be corrected for in Section 3.4.

3.2 Subtraction of the delayed neutron background

Delayed neutron decay was studied in one of our assemblies (lattice pitch $d = 16\cdot8$ cm, effective core height $H = 240$ cm). The detector position was at half the core height, channel width $\Delta t = 1\cdot28$ msec, repetition rate 2 per sec. The pulsed source was in operation 5 min before the experiment was started. The effective time constant of the delayed neutron decay was found to be $\alpha'' = 0\cdot40 \pm 0\cdot05$ sec^{-1}, which is in good agreement with the theoretical value $\alpha'' = \bar{\lambda} = 0\cdot407$ sec^{-1} resulting from equation (1.3) for $\rho \gg \beta$.

Figure 3 shows the thermal neutron flux decay $\phi(t)$ in the same assembly, obtained with a smaller channel width ($\Delta t = 0\cdot64$ msec) and a higher repetition rate (10 per sec) as in later experiments. For the prompt neutron part, there is no region showing an undisturbed exponential decay from which a determination of the fundamental mode decay constant α would be possible. We have a considerable admixture of higher harmonics in the region $t < 15$ msec and, on the other hand, delayed neutron contribution for $t > 15$ msec.

First of all, the delayed neutron effect has to be eliminated. It varies by less than 4 per cent according to previous experiments, within a 100 msec timing cycle and may be considered as a constant background to be subtracted from the neutron flux. The background intensity is determined from the background channel of the time analyser as illustrated in Section 2.3. The prompt neutron flux $\phi(t)$ corrected in this way is presented in Fig. 3. For $t > 15$ msec, we have an undisturbed exponential decay by more than one flux decade from which we obtain the fundamental mode decay constant $\alpha = 209$ sec^{-1}.

3.3 Separation of flux harmonics

In order to improve the accuracy of the method it is desirable to eliminate the contribution of higher modes present in the earlier part of the flux decay curve.
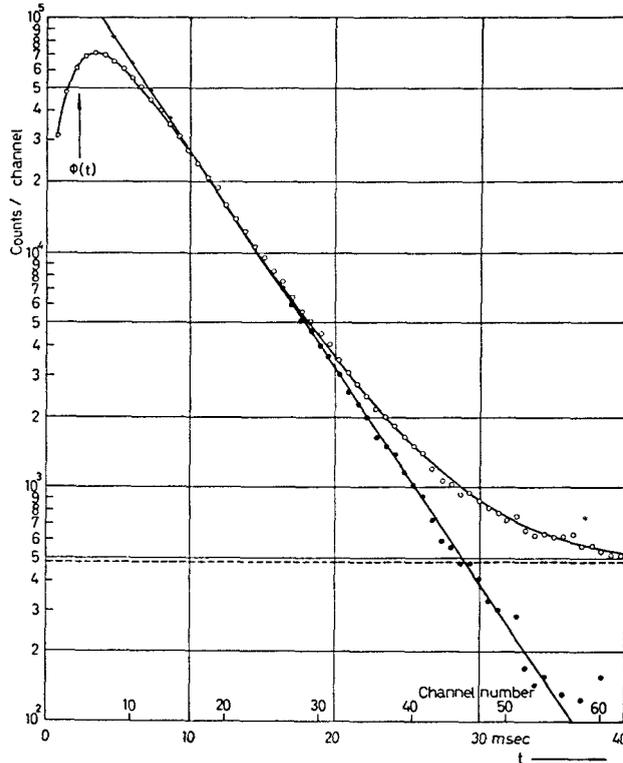
FIG. 3.—Thermal neutron flux decay at $z = H/2$.
($d = 16\cdot8$ cm, $H = 240$ cm, repetition rate 10 per sec.)
○ uncorrected; ✕ corrected for higher harmonics; ● corrected for background; – – – background intensity.

Therefore, during the following experiments the neutron flux was measured at several equidistant positions on the central axis in order to make a separation of axial flux harmonics possible.

Let us first consider the thermal neutron flux distribution $\phi(r, \varphi, z, t)$ in our assembly. Neglecting the small influence of the bottom reflector zone, the spatial dependence of ϕ with a buckling B^2 will be governed by the equation

$$\Delta\phi + B^2\phi = 0. \tag{3.1}$$

Assuming $\phi = 0$ as a boundary condition on the surface of a cylinder of the effective radius R and core height H, the flux ϕ may be written as an expansion of eigenfunctions φ_{klm}

$$\phi(r, \varphi, z, t) = \sum_{klm}^{\infty} A_{klm} \, \varphi_{klm}(r, \varphi, z) \cdot e^{-\alpha_{klm}t} \tag{3.2}$$

where

$$\varphi_{klm}(r, \varphi, z) = J_m(\mu_{lm}r) \cos m\varphi \sin \frac{k\pi z}{H}. \tag{3.3}$$

The radial eigenvalue μ_{lm} is determined by $\mu_{lm} = \nu_{lm}/R$, while ν_{lm} is the l-th zero of the Bessel function $J_m(\nu)$.

Each of the modes φ_{klm} dies out with an appropriate decay constant α_{klm} given by two-group theory in equation (4.7) assuming $l = 0$

$$\alpha_{klm} = \frac{1 + L^2B^2_{klm} - k_\infty(1 - \beta)/(1 + \tau B^2_{klm})}{l_2} \tag{3.4}$$

which depends on the geometrical buckling

$$B_{klm}{}^2 = k^2 \left(\frac{\pi}{H}\right)^2 + \left(\frac{\nu_{lm}}{R}\right)^2 \tag{3.5}$$

of the flux mode concerned.

The distribution of α_{klm} for one of our assemblies ($d = 16\cdot8$ cm, $H = 240$ cm, $R = 70\cdot3$ cm) is illustrated in Fig. 4, where the decay constants α_{klm} of various modes are arranged according to their axial index k. For an experimental determination of the fundamental mode decay constant, α_{100}, the most serious influence originates from the subsequent axial harmonics. For our specific tank geometry these modes are closely spaced in α as well as strongly excited due to the target position below the bottom of the tank The higher azimuthal modes ($m > 0$), on the contrary, are eliminated by the central detector position, while the higher radial modes ($l > 0$) are weakly excited as a
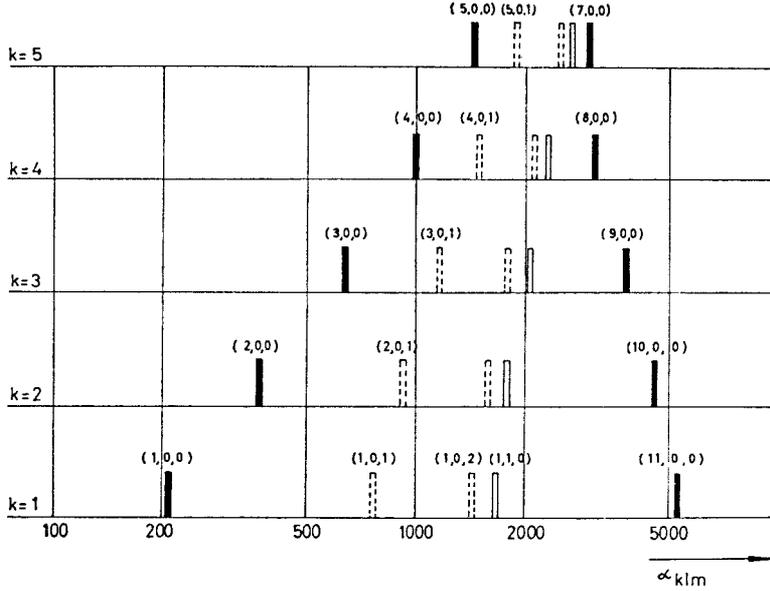
FIG. 4.—Distribution of modal decay constants α_{klm}, arranged according to axial index k. (Tank radius $R = 70{\cdot}3$ cm, $H = 240$ cm, $d = 16{\cdot}8$ cm.)

consequence of proper target adjustment. From this it is suggested to make use of a Fourier analysis procedure for separating axial harmonics.

The axial flux distribution given by equation (3.2) is written

$$\phi(z, t) = \sum_{k=1}^{\infty} A_k(t) \sin \frac{k\pi z}{H}; \ A_k(t) = \sum_{l=0}^{\infty} A_{kl0} e^{-\alpha_{klo} t} \quad (3.6)$$

If one determines the Fourier coefficients

$$A_k(t) = \frac{2}{H} \int^H \phi(z, t) \sin\frac{k\pi z}{H} \, dz \quad (k \geqslant 1) \quad (3.7)$$

from the experimental axial flux distribution $\phi(z, t)$ one has, within a region of negligible contribution of higher radial modes,

$$A_k(t) = A_{k00} \, e^{-\alpha_{k00} t}. \quad (3.8)$$

Hence, by plotting A_k vs. t it is easy to determine the decay constants α_{k00} of axial harmonics of various k.

In practice, the integral of equation (3.7) must be replaced by a sum over $N - 1$ equidistant abscissae. Instead of the coefficient $A_k(t)$ we obtain

$$A_k^*(t) = \frac{2}{N} \sum_{n=1}^{N-1} \phi(z_n, t) \cdot \sin \frac{kn\pi}{N} \ , \ (z_n = \frac{n}{N}H). \quad (3.9)$$

Bearing in mind that

$$\frac{2}{N} \sum_{n=1}^{N-1} \sin \frac{k'n\pi}{N} \cdot \sin \frac{kn\pi}{N} = \begin{cases} +1 \ (k' = k \bmod 2N) \\ -1 \ (k' = -k \bmod 2N) \\ \ \ 0 \ \ \text{otherwise} \end{cases}$$

we have the relation

$$A_k^*(t) = A_k(t) - A_{2N-k}(t) + A_{2N+k}(t)$$
$$- A_{4N-k}(t) + \dots . \quad (3.10)$$

The value $A_k^*(t)$ obtained in this way includes just as well contributions of particular higher Fourier coefficients $A_{2jN \pm k}$ in addition to the $A_k(t)$ wanted. As may be seen from equation (3.10) the competing axial modes $(2jN \pm k, 0, 0)$ are so much the farther, the higher the number $N - 1$ of detector positions employed.

3.4 Effect of the bottom reflector

Now, we consider the influence of the bottom reflector zone on the axial flux distribution in our assemblies. A small flux bump is to be expected at the boundary between core and reflector region, as well as some change in the axial buckling $\mu_z^2 = k^2\pi^2/H^2$ we are mostly interested in. According to perturbation theory this buckling change is a higher-order effect proportional to the third power of the reflector thickness.

Let us designate by h_c the height of the core region and by h_0 the reflector thickness, both including the extrapolation length at the outer surface of the region, as it is illustrated in Fig. 5. According to two-group theory equation (4.8) the axial distribution of fast and slow neutron fluxes, ϕ_1, ϕ_2, may be written in the core region ($z' > 0$)

$$\phi_1(z') = a_1 \sin \mu_z (h_c - z') + b_1 \sinh \nu_z (h_c - z')$$

$$\times \phi_2(z') = a_1 S_\mu \sin \mu_z (h_c - z') + b_1 S_\nu \sinh \nu_z (h_c - z')$$
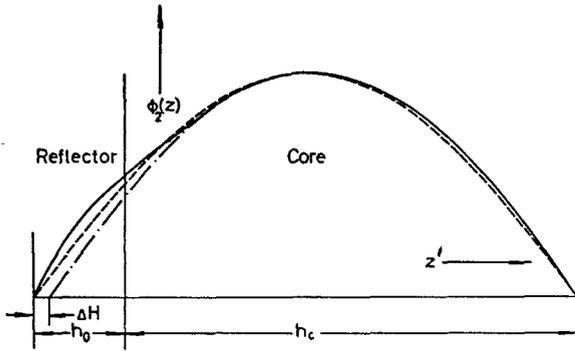$$(3.11)$$

FIG. 5.—Axial distribution of thermal neutron flux $\phi_2(z)$ - - - Unreflected tank; ——— Bottom reflector present; —·—· Asymptotic flux.

and in the heavy water reflector $(z' < 0)$

$$\phi_1(z') = b_2 \sinh \nu_z'(z' + h_0)$$

$$\phi_2(z') = a_2 \sin \mu_z'(z' + h_0) + b_2 S' \sinh \nu_z'(z' + h_0),$$
(3.12)

while $\mu_z^2 + \mu_r^2$ and $-\nu_z^2 + \mu_r^2$ are the roots of the characteristic equation (4.6) for the buckling B^2. Correspondingly, we have in the D_2O reflector

$$\mu_z'^2 + \mu_r^2 = -1/L'^2 + \alpha/v_2 D'_2$$

$$- \nu_z'^2 + \mu_r^2 = -1/\tau'.$$

A continuity condition at the boundary $z' = 0$ must be fulfilled by the flux ϕ as well as the current $D\dfrac{\partial\phi}{\partial z}$ of both neutron groups. Assuming equal decay constants α in both media we finally obtain

the axial index k of the mode and varies from $+1\cdot1$ per cent down to $-2\cdot2$ per cent, corresponding to a change of the effective core height ΔH by $-1\cdot1$ cm up to $2\cdot3$ cm which is small compared with the full core height $H_0 = 240$ cm.

TABLE 2.—EFFECT OF THE BOTTOM REFLECTOR
(Reflector thickness $h_0 = 22$ cm, $d = 16\cdot8$ cm.)

	Two media			Perturbation theory
k	$\Delta\mu_z^2$ (m^{-2})	$\Delta\mu_z^2/\mu_{z0}^2$	ΔH (cm)	$\Delta\mu_z^2$ (m^{-2})
$H = 240$ cm:				
1	$+0\cdot016$	$+0\cdot0096$	$-1\cdot15$	$+0\cdot011$
2	$+0\cdot027$	$+0\cdot0040$	$-0\cdot48$	$+0\cdot010$
3	$-0\cdot097$	$-0\cdot0063$	$+0\cdot77$	$-0\cdot088$
4	$-0\cdot400$	$-0\cdot0146$	$+1\cdot75$	$-0\cdot364$
$H = 210$ cm:				
1	$+0\cdot027$	$+0\cdot0106$	$-1\cdot11$	$+0\cdot019$
2	$+0\cdot017$	$+0\cdot0019$	$-0\cdot20$	$-0\cdot005$
3	$-0\cdot213$	$-0\cdot0106$	$+1\cdot11$	$-0\cdot209$
4	$-0\cdot795$	$-0\cdot0222$	$+2\cdot33$	$-0\cdot696$

Caused by this dependence on k, there is an unharmonic behaviour of the axial flux modes which was disregarded, however, in the modal analysis method because of the smallness of the effect given in Table 2.

3.5 Measurements

Each of the lattice assemblies listed in Table 1 was investigated at two different D_2O levels which were adjusted to render effective core heights $H = 240$ and 210 cm. In each case, the prompt neutron flux

$$\frac{\tan \mu_z h_c}{\mu_z} = \frac{-[(1 - \sigma')\nu_z' + (1 - \sigma)\nu_z \tanh \nu_z'h_0]\tan\mu_z' h_c/\mu_z' + (\sigma' - \sigma)\tanh \nu_z'h_0}{[(1 - \sigma)\nu_z' + (1 - \sigma')\nu_z \tanh \nu_z'h_0] + (\sigma' - \sigma)\nu_z'\nu_z\tan\mu_z'h_c/\mu_z'}$$
(3.13)

$(\sigma = S\nu/S\mu, \ \sigma' = S'/S\mu$ according to equation (4.9), $S' = \dfrac{D_1'}{D_2'}\dfrac{1}{1 + \tau'B'^2}$ for D_2O) from which the axial buckling μ_z^2 of the asymptotic flux may be determined.

Starting from the flux distribution in the unreflected tank of effective height $H_0 = h_c + h_0$ with $\mu_{z0} = k\pi/H_0$, as a first approximation, the change of axial buckling $\Delta\mu_z^2 = \mu_z^2 - \mu_{z0}^2$ caused by the reflector was calculated from equation (3.13) by an iterative process. For our particular geometry ($h_c = 218$ cm, $h_0 = 22$ cm, lattice pitch $d = 16\cdot8$ cm), Table 2 lists the buckling change $\Delta\mu_z^2$ as well as the relative effect $\Delta\mu_z^2/\mu_{z0}^2$ for the four lowest axial modes, $k \leqslant 4$. For comparison, results of a simple perturbation theory treatment analogous to that of Section 6.4 are included. Obviously, the effect $\Delta\mu_z^2/\mu_{z0}^2$ depends on

decay $\phi(z, t)$ was measured at 5 equidistant positions on the central axis using the same BF_3-counter consecutively. For normalization of source intensity the analyser data were related to the counting rate of a second BF_3-counter inside the lattice which determined the duration of an individual run by preset count operation (Fig. 1). The absolute source strength varied by less than 5 per cent during a typical series of measurements, while the normalized data of different runs were reproducible better than $0\cdot5$ per cent.

For one of the assemblies ($d = 16\cdot8$ cm, $H = 240$ cm), Fig. 6 presents the experimental flux decay $\phi(z_i, t)$ at various detector positions z_i corrected for background neutrons and dead time effects (channel width $\Delta t = 0\cdot32$ cm, repetition rate 10 per sec). In Fig. 7, the axial flux distribution $\phi(z, t)$ is shown at
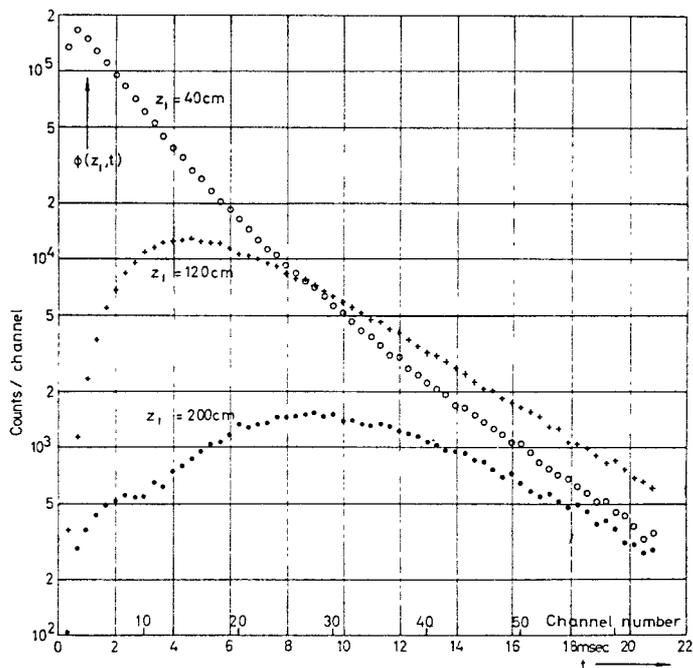
Fig. 6.—Thermal neutron flux decay $\phi(z_i, t)$ at different
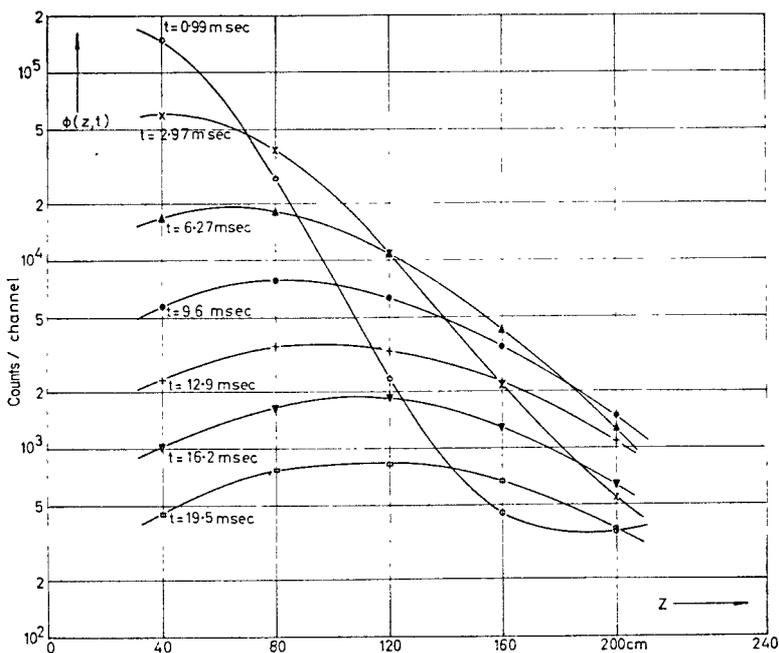detector positions z_i. ($d = 16\cdot8$ cm, $H = 240$ cm.)

Fig. 7.—Axial flux distribution $\phi(z, t)$ at different times t
after injection of source pulse. ($d = 16\cdot8$ cm, $H = 240$ cm.)

different time t. Immediately after the neutron burst injection ($t = 0.99$ msec), we have a highly asymmetrical flux distribution with its maximum near the bottom of the tank which changes over into the symmetrical fundamental mode within some 10^{-2} sec. In the plots for $t = 0.99$ msec (Fig. 7) and $z_i = 200$ cm (Fig. 6) a contribution of backscattered source neutrons incident into the top region of the tank may be seen. Hence, there is some influence on the excitation of flux modes but no proper change in the modes, since the backscattered neutron intensity dies out within about 100 μsec.

Because an accurate positioning of the BF_3-counter is important in these experiments, the effective boundaries of the axial flux must be known precisely. By flux measurements the extrapolation distance at the top surface was found to be 3.0 cm, which is larger than the $0.71 \lambda_t = 1.8$ cm assumed at the bottom reflector surface, owing to a Perspex cover plate on top of the assembly. From pulsed experiments using a larger channel width ($\Delta t = 0.64$ msec) the axial distribution of the fundamental mode was derived by adding up the last channels ($nr.$ 35–50) of the decay curves. A low contribution of the second axial harmonic that was still present was subtracted ($A_2/A_1 = 0.03$ according to Fig. 8). The experimental points agree well with the cos $\mu_z z$-curve, indicating that the detector positions were correctly arranged and no flux distortions caused by the bottom reflector zone are present at the lowest detector position.

From the experimental data we computed the Fourier coefficients $A_1^*(t)$ up to $A_5^*(t)$ applying equation (3.9) to each channel. A typical plot of $A_k^*(t)$ vs. t is given in Fig. 8. In the region $t > 3$ msec, the data of A_1^*, A_2^*, and A_3^* constitute an undisturbed exponential decay within almost two flux decades from which. the modal decay constants $\alpha_k = \alpha_{k00}$ were determined graphically. In the region $t < 3$ msec, however, there are deviations caused by higher radial modes as well as competing axial modes given by equation (3.10) and, to a lower extent, caused by thermalization effects. As may be seen from the
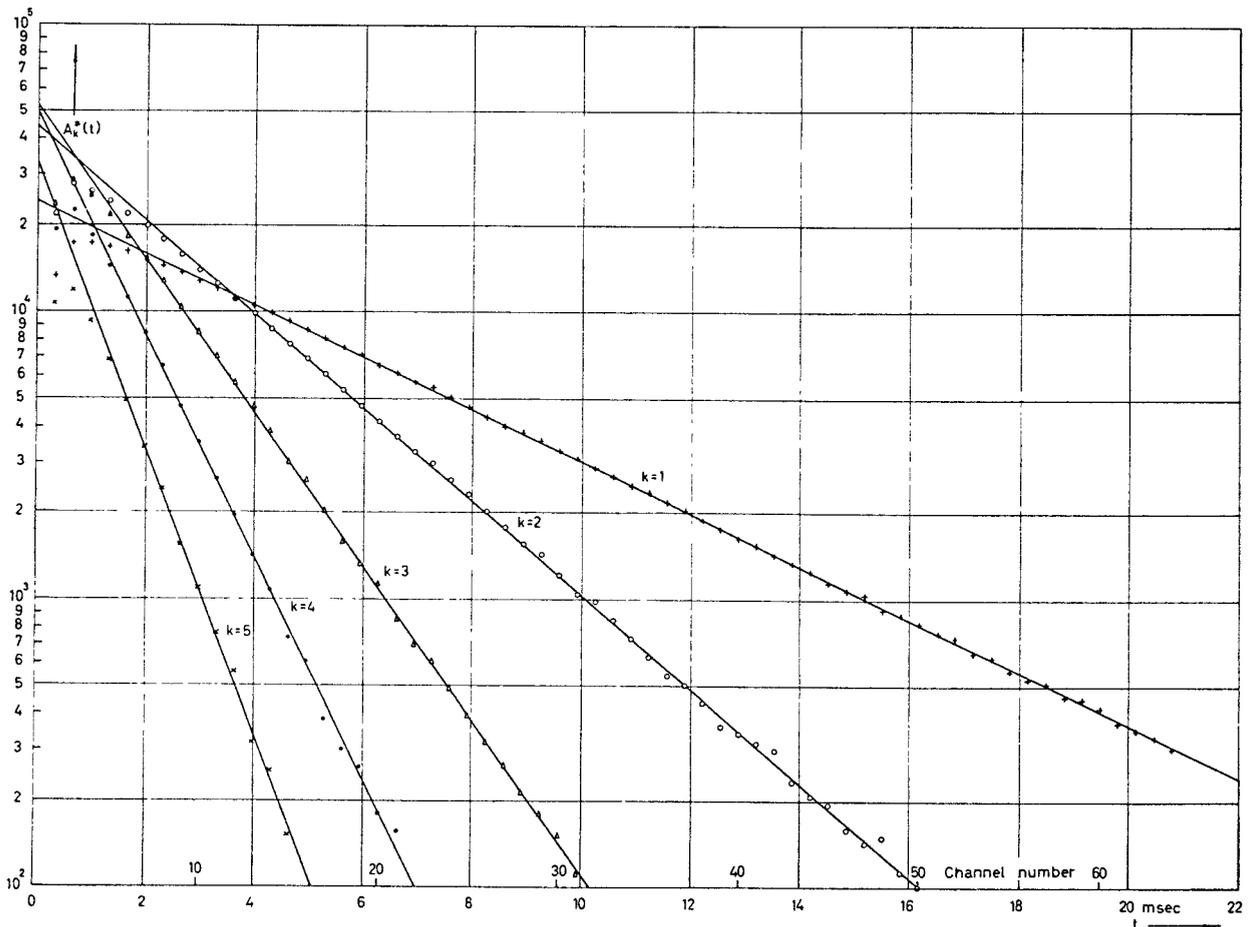

FIG. 8.—Decay of axial Fourier coefficients $A_k^*(t)$. ($d = 16.8$ cm, $H = 240$ cm.)

TABLE 3.—EXPERIMENTAL DECAY CONSTANT α AS A FUNCTION OF B^2
(k = index of axial harmonic).

| | $d = 15\cdot6$ cm | | $d = 16\cdot8$ cm | | $d = 18\cdot0$ cm | | $d = 21\cdot6$ cm | |
| | B^2 (m^{-2}) | α (sec^{-1}) | B^2 (m^{-2}) | α (sec^{-1}) | B^2 (m^{-2}) | α (sec^{-1}) | B^2 (m^{-2}) | α (sec^{-1}) |
k								
1	13·33	206 ± 1	13·33	207 ± 1	13·33	209 ± 1	13·32	223 ± 1
1	13·87	227 ± 2	13·87	225 ± 2	13·87	224 ± 2	13·86	237 ± 2
2	18·46	383 ± 4	18·48	375 ± 4	18·48	370 ± 4	18·48	365 ± 4
2	20·56	452 ± 6	20·57	438 ± 6	20·55	430 ± 6	20·54	421 ± 6
3	26·90	644 ± 10	26·92	623 ± 10	26·94	614 ± 10	26·96	586 ± 10
3	31·48	760 ± 16	31·53	745 ± 16	31·55	705 ± 16	31·61	680 ± 16
4	38·5	911 ± 50	38·6	919 ± 45	38·7	872 ± 45	38·8	848 ± 45
4	46·5	1012 ± 90	46·6	1050 ± 80	46·7	993 ± 80	46·9	970 ± 80

scattering of the experimental points, the standard deviation of $A_k^*(t)$ increases strongly with the index k of the mode. In addition, the difference in the α-values of A_k and the competing mode A_{2N-k} decreases rapidly with k (Fig. 4), so that the data of $α_4$ and $α_5$ are not very significant.

The resulting decay constants $α_k$ are listed in Table 3 with experimental errors derived from the scattering of the A_k^*-data, including a systematic error originating from an 0·5 per cent normalization inaccuracy. A small correction on α was made for the neutron absorption in the BF$_3$-counter and the central aluminium tube. From pulsed experiments employing the method of Section 6.1 an additive correction term $Δα = -2$ sec^{-1} was found.

The corresponding geometric buckling of the mode

$$B^2 = \mu^2 + k^2\pi^2/H^2 + \Delta\mu_z^2 \qquad (3.14)$$

is based on a radial buckling

$$\mu^2 = 11\cdot60 \pm 0\cdot12 \text{ m}^{-2}$$

which was obtained by radial flux measurements (MEISTER, 1961) for the lattice pitch $d = 16\cdot8$ cm. The small dependence of μ^2 on the lattice pitch as well as the difference between the static and dynamic flux distribution may be neglected here. The correction term $\Delta\mu_z^2$ for the axial reflector effect was taken from Table 2.

Finally, in Figs. 9–11 the time constant α is plotted against B^2 in order to be compared with theory.

4. TWO-GROUP MODEL

In order to describe prompt-neutron time behaviour we employ ordinary homogeneous two-group theory (GLASSTONE and EDLUND, 1957b). If the system is far from critical, $\rho \gg \beta$, as it is in our experiments, the prompt neutron part decays very fast compared with the delayed one. The latter, therefore, may be treated as a constant background which is assumed to be subtracted in the following considerations.

In this case, the fast neutron flux $\phi_1(\mathbf{r}, t)$ and the slow neutron flux $\phi_2(\mathbf{r}, t)$ are governed by

$$D_1 \cdot \Delta\phi_1 - \frac{D_1}{\tau} \cdot \phi_1 + k_\infty(1 - \beta) \cdot \frac{D_2}{L^2}\phi_2 = \frac{1}{v_1} \cdot \frac{\partial\phi_1}{\partial t}$$

$$D_2 \cdot \Delta\phi_2 - \frac{D_2}{L^2} \cdot \phi_2 + \frac{D_1}{\tau} \cdot \alpha_1 = \frac{1}{v_2} \cdot \frac{\partial\phi_2}{\partial t} \qquad (4.1)$$

where D_1, D_2 are the diffusion constants and v_1, v_2 the effective neutron velocities of the fast and thermal
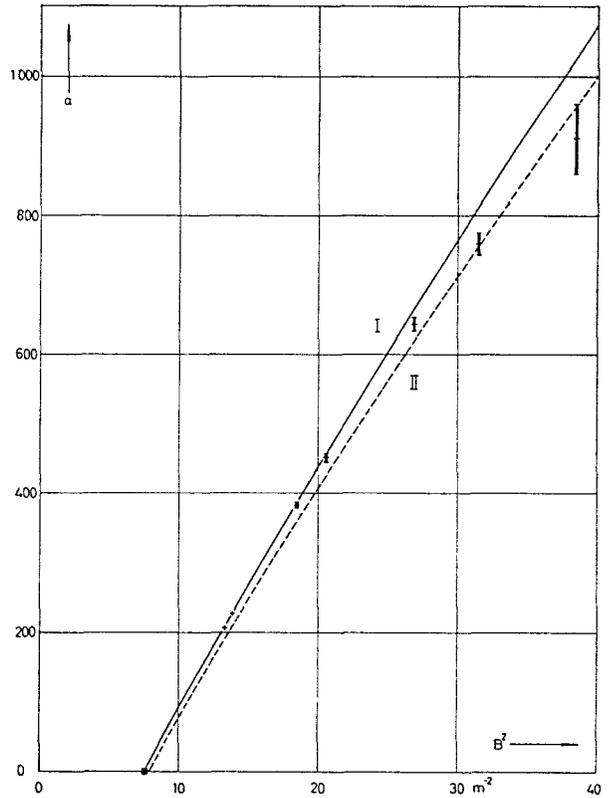

FIG. 9.—Prompt-neutron decay constant α vs. geometrical buckling B^2. ($d = 15\cdot6$ cm, $H = 240$ as well as 210 cm.)

⊥ Pulsed experiments; ■ Prompt critical buckling obtained in exponential experiments (MEISTER); ——— Two-group theory with reactor spectrum; — — — Two-group theory with Maxwellian spectrum.

FIG. 10.—Prompt-neutron decay constant α vs. geometrical buckling B^2. ($d = 16 \cdot 8$ cm, $H = 240$ as well as 210 cm.) $\frac{\tau}{\underline{\bot}}$ Pulsed experiments; ■ Prompt critical buckling obtained in exponential experiments (MEISTER); ——— Two-group theory with reactor spectrum; – – – – Two-group theory with Maxwellian spectrum.
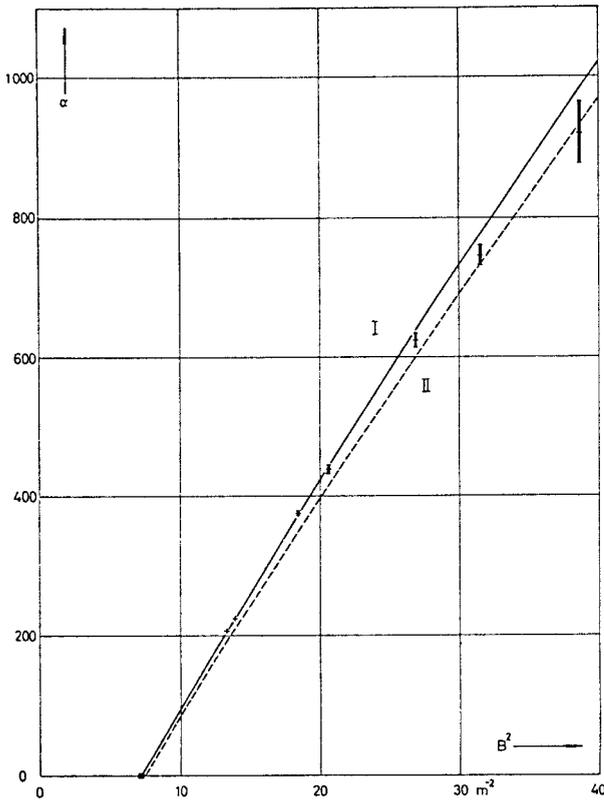
group, respectively, τ being the Fermi age of fission neutrons, L^2 the thermal group diffusion area, while $k_\infty(1 - \beta)$ is the prompt neutron multiplication factor of the medium.

There are solutions of equation (4.1) of the exponential type

$$\phi_{1,2}(\mathbf{r}, t) = \phi_{1,2}(\mathbf{r})e^{-\alpha t} \qquad (4.2)$$

having a space dependence according to

$$\Delta\phi_{1,2}(\mathbf{r}) + B^2\phi_{1,2}(\mathbf{r}) = 0 \qquad (4.3)$$

where B^2 is the buckling of the flux distribution. Hence, we obtain from equation (4.1)

$$-(1 + \tau B^2 - \alpha l_1)\phi_1 + k_\infty(1 - \beta) \cdot \frac{\tau}{L^2} \cdot \frac{D_2}{D_1} \cdot \phi_2 = 0$$

$$\frac{L^2}{\tau} \cdot \frac{D_1}{D_2} \cdot \phi_1 - (1 + L^2 B^2 - \alpha l_2)\phi_2 = 0 \qquad (4.4)$$

where

$$l_1 = \tau/v_1 D_1, \qquad l_2 = L^2/v_2 D_2 \qquad (4.5)$$

are the infinite medium neutron lifetimes of each group.

From equation (4.4) we get the relation between buckling B^2 and the decay constant α as follows:

$$(1 + L^2 B^2 - \alpha l_2)(1 + \tau B^2 - \alpha l_1)$$
$$- k_\infty(1 - \beta) = 0. \qquad (4.6)$$

For each B^2 we obtain from this two values of α which may be written in the case $l_1/l_2 \ll 1$

$$\alpha' \approx \frac{1 + \tau B^2}{l_1} + \frac{k_\infty (1 - \beta)}{l_2(1 + \tau\beta^2)}$$

$$\alpha \approx \frac{1 + L^2 B^2}{l_2} - \frac{k_\infty(1 - \beta)}{l_2(1 + \tau B^2 - \alpha l_1)} \qquad (4.7)$$

α' being the time constant of the slowing down process and α the decay constant of the asymptotic thermal neutron spectrum. On the other hand, there are two solutions of B^2 for each α, that is, besides B^2 as well

$$B'^2 = -B^2 - \frac{1 - \alpha l_1}{\tau} - \frac{1 - \alpha l_2}{L^2}.$$
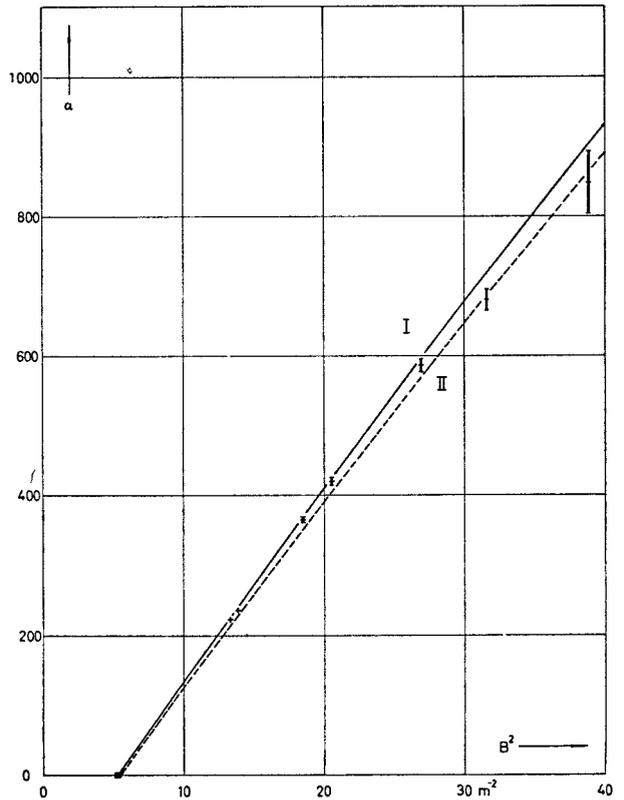
FIG. 11.—Prompt-neutron decay constant α vs. geometrical buckling B^2. ($d = 21 \cdot 6$ cm, $H = 240$ as well as 210 cm.) $\frac{\tau}{\underline{\bot}}$ Pulsed experiments; ■ Prompt critical buckling obtained in exponential experiments (MEISTER); ——— Two-group theory with reactor spectrum; – – – – Two-group theory with Maxwellian spectrum.

Consequently, the solution of equation (4.1) may be written in the one-dimensional case as follows

$$\phi_1(z, t) = \{a \sin \mu z + b \sinh \nu z\}e^{-\alpha t}$$
$$+ c \sin \mu z \cdot e^{-\alpha' t}$$
$$\phi_2(z, t) = \{aS_\mu \sin \mu z + bS_\nu \sinh \nu z\} e^{-\alpha t}$$
$$+ cS_\mu' \sin \mu z \cdot e^{-\alpha' t}$$
$$(\mu^2 = B^2; \quad \nu^2 = -B'^2). \tag{4.8}$$

The so-called transition term $\sinh \nu z$ only occurs if the boundary conditions of fast and thermal neutron flux are different, as in the case of a reflected system, in order to allow a spatial matching of neutron spectra.

The coupling coefficients S_μ, S_ν, S_μ', relating fast and thermal part of the solution are given by means of equation (4.4):

$$S_\mu = \frac{L^2}{\tau} \cdot \frac{D_1}{D_2} \cdot \frac{1 + \tau B^2 - \alpha l_1}{k_\infty(1 - \beta)}$$

$$S_\nu = -\frac{D_1}{D_2} \cdot \frac{1}{1 + \tau B^2 - \alpha l_1}$$

$$S_\mu' = -\frac{v_2}{v_1} \cdot \frac{1}{1 + \tau B^2} . \tag{4.9}$$

5. COMPARISON OF EXPERIMENTS WITH TWO-GROUP THEORY

For comparison with our experimental data the prompt neutron decay constant α was calculated by homogeneous two-group theory employing the iterative formula

$$\alpha = \frac{1}{l_2} + v_2 D_2 B^2 - \frac{k_\infty(1 - \beta)}{l_2(1 + \tau B^2 - \alpha l_1)} \tag{5.1}$$

derived from equation (4.7). The effective lattice parameters involved in equation (5.1) were partly taken from exponential experiments (MEISTER, 1961) partly they were computed from nuclear cross-section data as is illustrated in the following sections.

5.1 Thermal group constants

If the number of lattice cells in a heterogeneous assembly is sufficiently high, it may be treated as a homogeneous medium having effective cross sections, Σ_a, Σ_{tr}, which are usually defined by spatial flux weighting of material cross sections over a lattice cell.

The effective absorption cross section obtained by this concept is

$$\Sigma_a = \Sigma_U \frac{V_U \, \bar{\varphi}_U}{V_M \, \bar{\varphi}_M} \cdot \frac{1}{f} \left(1 + \frac{V_U \, \bar{\varphi}_U}{V_M \, \bar{\varphi}_M} \right.$$
$$\left. + \frac{V_{AL} \, \bar{\varphi}_{AL}}{V_M \, \bar{\varphi}_M} \right)^{-1} \tag{5.2}$$

where f is the thermal utilization, $\bar{\varphi}_i$ the average microscopic thermal flux in region i of partial volume V_i, i indicating uranium, aluminium, and D_2O-moderator, respectively. The data used for computing Σ_a, as listed in Table 4, were taken from exponential experiments (MEISTER, 1961) except for the absorption cross section Σ_U of natural uranium to be considered later on.

By the same procedure, the effective transport cross section turns out to be almost equal to the moderator value, $\Sigma_{tr} \approx \Sigma_M$, since the volume fraction of U and Al in a lattice cell is less than 0·05 and the transport cross sections of U and D_2O are nearly equal. Therefore, we have for the effective diffusion constant $D = 1/3\Sigma_{tr}$

$$D = D_M. \tag{5.3}$$

As the next step, we take into consideration the energy dependence of Σ_a and D. As may be seen from the derivation of the two-group theory, Σ_a as well as D have to be averaged over the energy spectrum $\phi(E)$ of the thermal neutron flux

$$\langle \Sigma_a \rangle = \frac{\int_0^{E_1} \Sigma_a(E)\phi(E) \, dE}{\int_0^{E_1} \phi(E) \, dE} \ ; \ \langle D \rangle = \frac{\int_0^{E_1} D(E)\phi(E) \, dE}{\int_0^{E_1} \phi(E) \, dE} \tag{5.4}$$

where E_1 is a proper limiting energy of the thermal group. For a pure Maxwellian spectrum of temperature T and a $1/v$ cross section, for instance, we have the well-known relation

$$\langle \Sigma_a \rangle = \frac{\sqrt{\pi}}{2} \Sigma_a(kT) .$$

In our assemblies, however, there are appreciable deviations from a $1/v$-dependence as well as from a pure Maxwellian spectrum. Therefore, $\langle \Sigma_a \rangle$ and $\langle D \rangle$

TABLE 4.—LATTICE PARAMETERS OBTAINED IN EXPONENTIAL EXPERIMENTS

d (cm)	$B_m{}^2$ (m^{-2})	$V/_M V_U$	φ_M/φ_U	f	k_∞
15·6	8·04 ± 0·13	29·09	1·960	0·980 ± 0·001	1·229 ± 0·010
16·8	7·65 ± 0·13	33·93	1·988	0·978 ± 0·001	1·239 ± 0·010
18·0	7·15 ± 0·16	39·12	2·015	0·976 ± 0·001	1·245 ± 0·011
21·6	5·66 ± 0·16	56·85	2·097	0·968 ± 0·002	1·252 ± 0·012

were computed by numerical integration on the basis of equation (5.4) using nuclear cross sections of ^{238}U (WEINBERG and WIGNER, 1958)

$$\sigma_a(E) = 2\cdot73 \sqrt{\frac{E_0}{E}} \left\{ 1 + \frac{1}{6\cdot8\ \text{eV}} (E - E_0) \right\} \text{ barns}$$

and of ^{235}U given in BNL-325 (HUGHES and SCHWARZ 1958). The energy dependence of the diffusion constant of D_2O was calculated according to the RADKOWSKY prescription (RADKOWSKY, 1950)

$$D_M(E) \sim \left[\sigma_0(E)\left(1 - \frac{2}{3A}\right) + 2\sigma_D(E)\left(1 - \frac{2}{3M_{eff}}\right) \right]^{-1}$$

with an effective mass $M_{eff}(E)$ given by

$$\left(\frac{M_{eff}}{1 + M_{eff}}\right)^2 = \sigma_D(E)/7\cdot65 \text{ barns}$$

and atomic scattering cross sections $\sigma_0(E)$, $\sigma_D(E)$, taken from BNL-325.

The neutron flux $\phi(E)$ was assumed to be the stationary thermal neutron spectrum as it was calculated by KUNZE (1962) on the basis of the heavy gas model for the moderator region of our lattices. The limiting energy was chosen $E_1 = 0\cdot4$ eV to be the effective Cd-cut-off energy of our stationary flux measurements (MEISTER, 1961).

The effective parameters $\langle \Sigma_a \rangle$, $\langle D \rangle$, and the effective thermal group velocity $v_2 = 1/\langle 1/v \rangle$, divided by the standard values at $v_0 = 2200$ m/sec, are plotted against the lattice pitch d in Fig. 12. In the case of $\langle \Sigma_a \rangle$ and $\langle 1/v \rangle$, there are deviations from the Maxwellian average as large as 8 per cent, while there are smaller deviations for $\langle D \rangle$.

From these data we finally derived the lattice parameters

$$l_2 = \frac{\langle 1/v \rangle}{\langle \Sigma_a \rangle} \qquad L_2 = \frac{\langle D \rangle}{\langle \Sigma_a \rangle} \qquad v_2 D_2 = \frac{\langle D \rangle}{\langle 1/v \rangle} \qquad (5.5)$$

to be used in equation (5.1), which are listed in Table 5. The value of $v_2 D_2$ is based on the Maxwellian average

$$(v_2 D_2)_{\text{Maxw}} = 2\cdot01 \,.\, 10^5 \text{ cm}^2/\text{sec}$$

$$- 4\cdot00 \,.\, 10^5 \text{ cm}^4/\text{sec} \,.\, B^2$$

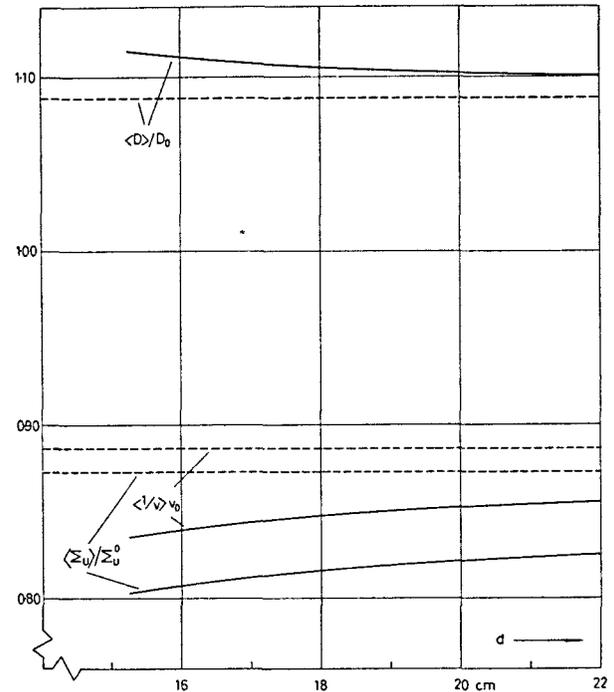
FIG. 12.—Effective cross sections divided by standard values at $v_0 = 2200$ m/sec as a function of lattice pitch d. ——— Reactor spectrum; – – – – Maxwellian spectrum.

which was obtained by the pulsed-neutron method for the D_2O used in our experiments (MEISTER, 1962). The small dependence on B^2 is caused by the diffusion cooling effect.

TABLE 5.—LATTICE PARAMETERS USED IN TWO-GROUP THEORY

d (cm)	$v_2 D_2$ (10^5 cm^2/sec)	l_2 (10^{-3} sec)	L^2 (cm^2)	l_1 (10^{-6} sec)	τ (cm^2)	$k_\infty (1 - \beta)$
Reactor spectrum:						
15·6	2·17	0·743	160·6	13·5	115	1·220
16·8	2·15	0·874	187	13·5	115	1·230
18·0	2·13	1·018	216	13·5	115	1·236
21·6	2·10	1·510	317	13·5	115	1·243
Maxwellian spectrum:						
15·6	2·01	0·752	151·1	13·5	115	1·220
16·8	2·01	0·880	176·9	13·5	115	1·230
18·0	2·01	1·023	205	13·5	115	1·236
21·6	2·01	1·512	304	13·5	115	1·243

5.2 Fast group constants

In a consistent two-group theory, the slowing down area is defined by

$$\tau = \frac{\int_{E_1}^{E_f} D(E)\phi(E)\,\mathrm{d}E}{\int_{E_1}^{E_f}\mathrm{d}E'\int_{0}^{E_1}\mathrm{d}E\,\Sigma(E'\to E)\phi(E')} \qquad (5.6)$$

$\Sigma(E'\to E)$ being the transfer cross section and E_f an effective upper energy limit given by fission neutron energies. For elastic collisions with free nuclei assuming a $1/E$ slowing down spectrum and energy-independent D, this definition is identical with the well-known Fermi age formula

$$\tau = \int_{E_1}^{E_f}\frac{D(E)}{\xi\Sigma_s(E)}\cdot\frac{\mathrm{d}E}{E}. \qquad (5.7)$$

The effective Fermi age τ of the lattice was calculated from the moderator value τ_M, taking into account the inelastic scattering in the uranium and the dilution of the moderator (MEISTER, 1961). For our specific lattice geometry, $d = 15\cdot6$ to $21\cdot6$ cm, we have within ± 1 per cent

$$\tau = \tau_M.$$

The Fermi age of fission neutrons in D_2O down to $E_1 = 0\cdot4$ eV was assumed to be $\tau_M = 115$ cm^2, based on an experimental age $\tau_{1\cdot44} = 109$ cm^2 (WADE, 1956) down to indium resonance energy.

The infinite medium mean lifetime of fast group neutrons is given by

$$l_1 = \frac{\tau}{v_1 D_1}\ ; \qquad \frac{1}{v_1} = \frac{\int_{E_1}^{E_f}\frac{1}{v}\,\phi(E)\,\mathrm{d}E}{\int_{E_1}^{E_f}\phi(E)\,\mathrm{d}E}. \qquad (5.8)$$

Assuming $E_1 = 0\cdot4$ eV, $E_f = 2$ MeV, and a $1/E$ slowing down spectrum we have $l_1 = 13\cdot5$ μsec in our lattices.

The infinite medium multiplication factor k_∞ has been determined from earlier material buckling measurements on the same lattice assemblies (MEISTER, 1961) employing the two-group equation $k_\infty = (1 + L^2 B_m^2)\cdot(1 + \tau B_m^2)$. Hence, we derived the prompt-neutron multiplication factor $k_\infty(1 - \beta)$ listed in Table 5 assuming $\beta = 0\cdot0075$.

Except for the multiplication factor k_∞, the two-group parameters considered so far, in principle, are dependent on the limiting energy E_1 which was arbitrarily chosen. The resulting decay constant α, however, must be independent of E_1, provided that

the correct solution $\phi(E)$ has been used as a weighting function in equations (5.4) and (5.6).

5.3 Discussion of the experimental results

In Figs. 9–11 the experimental α-values are compared with two-group theory, equation (5.1). First of all, $\alpha(B^2)$ was calculated with lattice parameters based on the stationary neutron spectrum which would be present, for instance, in a critical reactor, $B^2 = B_m^2$. As may be seen from curve (I) there is good agreement with experimental data in the lower buckling region, $B^2 < 20$ m^{-2}. For higher B^2, however, the experimental α-values are considerably lower than theoretical ones.

This discrepancy indicates that the lattice parameters, which were assumed to be constant so far, are rather a function of the geometric buckling B^2. In general, there are various effects leading to a B^2-dependence of this kind:

(a) A heterogeneous assembly of fuel rods, in principle, represents an anisotropic medium giving rise to anisotropic diffusion constants. Earlier experimental work, however, did not give any conclusive indication of anisotropic diffusion properties in a lattice without any cooling channels or voids.

Moreover, there may be a typical heterogeneous effect leading to a variation of the intracell flux distribution from which a B^2-dependence of the flux ratio $\bar{\varphi}_M/\bar{\varphi}_U$ as well as the lifetime l_2 would arise. On the basis of a one-velocity model some calculations were made using the P_1-approximation. The resulting variation of $\bar{\varphi}_M/\bar{\varphi}_U$ and l_2 turned out to be less than $0\cdot5$ per cent for our assemblies within the B^2-range covered by experiments which is to be neglected here.

Another heterogeneous effect originates from the non-ideal fitting of the square lattice into a cylindrical tank which results in an effective reflector zone at the boundary, in particular for our lattice pitch $d = 15\cdot6$ cm. By a perturbation theory treatment analogous to that of Section 6.4, however, this effect proved to be negligible.

(b) The Fermi age $\tau = 115$ cm derived from the second moment $\bar{r^2}$ of the spatial slowing down distribution (WADE, 1956) was assumed to be independent of B^2. The fast group non-escape probability

$$P(B^2) = \frac{1}{1 + \tau B^2} \qquad (5.9)$$

with a constant $\tau = \bar{r^2}/6$ used in the two-group theory is only the first approximation to the exact formula

$$P(B^2) = \sum_{n=0}^{\infty}\frac{(-1)^n}{(2n+1)!}\cdot\overline{r^{2n}}\cdot B^{2n} \qquad (5.10)$$

including higher moments $\overline{r^{2n}}$ as well. When using the two-group formula equation (5.9) instead of equation (5.10), an effective τ should be used which is also a function of B^2. This effect is supposed to have some influence on the $\alpha(B^2)$ curve; for an exact evaluation of equation (5.10), however, more accurate slowing down density curves for D$_2$O are needed.

(c) With increasing B^2, there is a shift of the asymptotic neutron spectrum $\phi(E)$ towards lower energies. First of all, the ratio of the spatially asymptotic parts of the fast and thermal neutron fluxes resulting from two-group theory, equation (4.9),

$$\frac{\int_0^{E_1} \phi(E)\, \mathrm{d}E}{\int_{E_1}^{E_f} \phi(E)\, \mathrm{d}E} = S_\mu \approx \frac{L^2}{\tau} \cdot \frac{D_1}{D_2} \cdot \frac{1 + \tau B^2}{k_\infty (1 - \beta)} \quad (5.11)$$

shows a systematic decrease of the slowing down part compared with the thermal component, if B^2 as well as α increase. This effect is caused by the leakage of fast neutrons out of the system.

In addition, there will be a diffusion-cooling effect in the thermal spectrum itself caused by the favoured leakage of the faster neutrons which results in a decrease of the average diffusion constant $v_2 D_2$, as it is known from a pure moderator. In a multiplying medium diffusion cooling will have also some influence on the other lattice parameters, e.g. l_2 and k_∞, in addition to $v_2 D_2$.

This influence may be calculated on the basis of a known diffusion-cooling constant C, if the neutron temperature coefficients of the lattice parameters are known:

$$\frac{\mathrm{d}l_2}{\mathrm{d}B^2} = \gamma\, \frac{\mathrm{d}l_2}{\mathrm{d}T}, \frac{\mathrm{d}k_\infty}{\mathrm{d}B^2} = \gamma\, \frac{\mathrm{d}k_\infty}{\mathrm{d}T}, \frac{\mathrm{d}v_2 D_2}{\mathrm{d}B^2} = \gamma\, \frac{\mathrm{d}v_2 D_2}{\mathrm{d}T} = -C.$$
$$(5.12)$$

However, it is open to some question if there will be the same diffusion-cooling constant in a multiplying system as in the pure moderator.

For higher B^2, no detailed information on neutron spectra in our assemblies is available. The only thing which can be stated is that for very high B^2 the neutron spectrum is expected to approach the moderator spectrum, since multiplication and absorption processes are overcome by thermal neutron leakage. Accordingly, a limiting function $\alpha(B^2)$ was calculated by equation (5.1) with lattice parameters (Table 5) based on a pure Maxwellian spectrum; the diffusion-cooling constant was considered to be equal to the moderator value, $C = 4\cdot0 \cdot 10^5$ cm^4/sec (MEISTER, 1962) and the temperature coefficients used in equation (5.12)

were

$$\frac{1}{k_\infty}\frac{\mathrm{d}k_\infty}{\mathrm{d}T} = -10^{-4}/°C; \frac{1}{l_2}\frac{\mathrm{d}l_2}{\mathrm{d}T} = -9.10^{-4}/°C;$$

$$\frac{1}{v_2 D_2}\frac{\mathrm{d}v_2 D_2}{\mathrm{d}T} = 22.10^{-4}/°C.$$

The variation of the lifetime l_2 mainly originates from a temperature dependence of the intracell flux ratio $\bar\varphi_M/\bar\varphi_U$ in equation (5.2) which is given by P_1-theory as follows:

$$\frac{\bar\varphi_U}{\bar\varphi_M}\frac{\mathrm{d}}{\mathrm{d}T}\frac{\bar\varphi_M}{\bar\varphi_U} = \frac{\bar\varphi_M/\bar\varphi_U - 1}{\bar\varphi_M/\bar\varphi_U}\frac{-1}{2T}.$$

In Figs. 9–11 the limiting curve (II) was plotted. The experimental points are seen to approach this curve in the region of higher geometrical buckling. Because of the experimental errors increasing strongly with B^2, however, no precise statements can be made on the magnitude of the diffusion-cooling constant in the lattice.

6. EFFECT OF LATTICE PERTURBATIONS

The reactivity contribution of single fuel elements as well as cadmium rods completely inserted into the lattice has been determined in some of the assemblies listed in Table 1 employing the pulsed method and the stationary exponential experiment for comparison.

As a measure of the reactivity effect in question, we consider the relative change of the radial buckling μ_0^2 of the undisturbed flux distribution

$$\phi_0(r) = A_0 J_0(\mu_0 r)$$

caused by inserting the sample. If the absorber is placed on the central axis of the assembly, for instance, the asymptotic part of the radial flux may be written

$$\phi(r) = A\{J_0(\mu r) + a Y_0(\mu r)\},$$

where the coefficient a of the perturbation term is determined by the strength q of an effective negative line source: $a = -q/4D\phi_0$. Assuming $\phi = 0$ on the boundary $(r = R)$ we obtain the buckling change $\Delta\mu^2 = \mu^2 - \mu_0^2$ to a first approximation

$$\frac{\Delta\mu^2}{\mu_0^2} = 2a \cdot \frac{Y_0(\mu_0 R)}{\mu_0 R\, J_1(\mu_0 R)} = 0\cdot817a. \quad (6.1)$$

Similar relations may be derived for eccentric absorbers.

6.1 Pulsed experiments

If an absorber rod is completely inserted parallel to the axis of the assembly, the total geometrical buckling

$$B^2 = \mu^2 + k^2\pi^2/H^2$$

of the flux distribution changes, due to the effect on the radial part, μ^2, whereas the axial part determined by

the core height H remains constant. Therefore, we have

$$\Delta\mu^2 = \Delta B^2. \qquad (6.2)$$

Since there is a definite relationship between B^2 and the decay constant α as given by experimental curves, for instance, ΔB^2 can be determined from the corresponding change of the prompt-neutron decay constant $\Delta\alpha$ caused by the absorber. Accordingly, from two-group theory equation (4.7) the relation

$$\Delta B^2 = \cfrac{\Delta\alpha}{v_2 D_2 \left\{ 1 + \cfrac{\tau k_\infty (1 - \beta)}{L^2 (1 + \tau B^2)^2} \right\}} \qquad (6.3)$$

may be derived.

6.2 Stationary experiments

The effect of axial lattice perturbations has been examined in connexion with exponential experiments as well. We used a 1 curie Ra-Be neutron source placed inside a graphite pedestal below the experimental tank (MEISTER, 1961).

The spatial decrease of the asymptotic neutron flux was measured on the central axis as in the undisturbed case

$$\phi_0(r, z) = A_0 J_0(\mu_0 r)\, e^{-\gamma_0 z}$$

as in the perturbed case

$$\phi(r, z) = A \{J_0(\mu r) + a Y_0(\mu r)\}\, e^{-\gamma z}.$$

The relation holds

$$\mu_0^2 - \gamma_0^2 = \mu^2 - \gamma^2 = B_m^2, \qquad (6.4)$$

i.e. the axial relaxation length of neutron flux comes out in such a way as to render its geometrical buckling equal to the material buckling B_m^2 of the multiplying medium. Hence, from the experimental axial buckling change $\Delta\gamma^2 = \gamma^2 - \gamma_0^2$ we may get the radial buckling effect

$$\Delta\mu^2 = \Delta\gamma^2 \qquad (6.5)$$

to be determined.

6.3 Effect of cadmium rods

First we examined the effect of cadmium rods of 2·3 and 4·7 cm diameter as a function of their radial position in the lattice. The absorber rod was successively placed at various positions (x, y) symmetrically surrounded by 4 neighbouring fuel elements. The central position was not accessible, since the neutron detector was placed there.

The cadmium rods in use were made of an aluminium tube (25 × 1 mm and 50 × 1·5 mm) sealed at the lower end into which a cylindrical cadmium sheet of 0·8 mm thickness was inserted. The inner volume of the rod was partially filled with an iron core

in order to allow the rod to be freely suspended in the heavy water moderator.

During most of our pulsed experiments we employed only one neutron detector position at half the core height for eliminating the second axial mode. Because of higher modes present in the earlier part, the flux decay curves were evaluated exclusively in the region $t > 12$ msec employing a proper delay time in the analyser.

The experimental flux decay $\phi(t) = A\, e^{-\alpha t}$ was related to the undisturbed flux $\phi_0(t) = A_0 e^{-\alpha_0 t}$ by plotting the ratio

$$\phi(t)/\phi_0(t) = \text{const. } e^{-\Delta\alpha t}$$

on a logarithmic scale against the time t. The values of $\Delta\alpha$ obtained from the slope of a straight line are presented in Table 6. By means of the experimental α vs. B^2 curves, Figs. 9 and 10, we determined the corresponding buckling change ΔB^2 in order to get $\Delta\mu^2/\mu_0^2$, as shown in Table 6. Furthermore, we listed the results of our stationary experiments for comparison. Within the limits of error which are somewhat larger in the stationary case, we have a good agreement between both methods, even though the geometrical buckling in the stationary state $(B^2 = B_m^2 \approx 7\cdot6 \text{ m}^{-2})$ and in the time-dependent case $(B^2 = 13\cdot3 \text{ m}^{-2})$ are quite different. One may conclude that there is only a weak dependence of $\Delta\mu^2/\mu_0^2$ on the buckling of the axial flux distribution.

In Figs. 13 and 14 $\Delta\mu^2/\mu_0^2$ of Cd-rods is plotted as a function of their distance r from the central axis. Assuming a relation of the type

$$\Delta\mu^2/\mu_0^2 = \text{const } [J_0(\mu_0 r)]^n \qquad (6.6)$$

we used $J_0(\mu_0 r)$ with $\mu_0^2 = 11\cdot6 \text{ m}^{-2}$ as an abscissa in order to determine the exponent n by linear interpolation. Instead of the value $n = 2$ expected from a one-group perturbation theory we get $n = 2\cdot15$ in comparison with $n = 2\cdot2$ found by PERSSON et al., (1958) in similar experiments. Finally, we determined the effect of a central rod by an extrapolation procedure on the basis of equation (6.6), as illustrated in Figs. 13 and 14.

A central cadmium rod of geometrical radius ρ is easily treated by two-group theory (GLASSTONE and EDLUND, 1957) resulting in

$$\frac{\Delta\mu^2}{\mu_0^2} = -0\cdot817$$

$$\times \frac{1}{\left\{ Y_0(\mu\rho) + d_2\mu Y_1(\mu\rho) - \cfrac{2}{\pi} \cdot \cfrac{S_r}{S_\mu} \cdot (K_0(\nu\rho) + d_2\nu K_1(\nu\rho)) \right\}} \qquad (6.7)$$

TABLE 6.—RADIAL BUCKLING EFFECT $\Delta\mu^2/\mu_0^2$ OF CADMIUM RODS
(ρ = radius of Cd-rod, r = distance from rod to central axis).

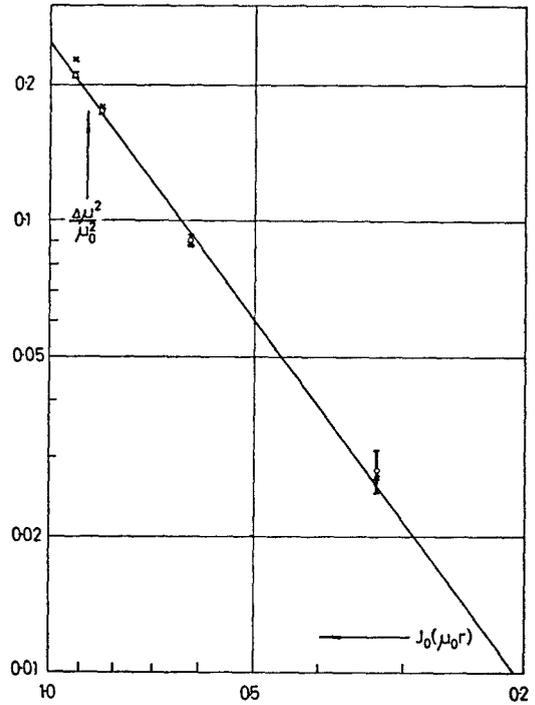| d (cm)	ρ (cm)	x	y	r (cm)	$\Delta\alpha$ (sec⁻¹)	$(\Delta\mu^2/\mu_0^2)$ Pulsed method	$(\Delta\mu^2/\mu_0^2)$ Exponential method
16·8	2·3	0	$1d$	16·8	54·9 ± 1·2	0·143 ± 0·003	0·132 ± 0·008
		$1d$	$1d$	23·8	44·4 ± 1·2	0·116 ± 0·003	0·126 ± 0·008
		$2d$	$1d$	37·6	24·7 ± 1·2	0·064 ± 0·003	0·059 ± 0·008
		$3d$	$1d$	53·1	7·8 ± 1·2	0·017 ± 0·003	0·024 ± 0·010
16·8	4·7	0	$1d$	16·8	81·6 ± 1·2	0·210 ± 0·003	0·229 ± 0·008
		$1d$	$1d$	23·8	68·0 ± 1·2	0·175 ± 0·003	0·177 ± 0·008
		$2d$	$1d$	37·6	34·9 ± 1·2	0·090 ± 0·003	0·089 ± 0·010
		$3d$	$1d$	53·1	10·8 ± 1·2	0·028 ± 0·003	0·027 ± 0·008
16·8	2·3	·5d	·5d	11·9	70·5 ± 1·5	0·181 ± 0·005	0·194 ± 8·008
	4·7	·5d	·5d	11·9	105·4 ± 1·5	0·271 ± 0·005	0·283 ± 0·008
15·6	2·3	0	$1d$	15·6	54·8 ± 1·5	0·134 ± 0·005	
		$1d$	$1d$	22·1	46·9 ± 1·5	0·113 ± 0·005	
		$2d$	$1d$	34·8	27·9 ± 1·5	0·066 ± 0·005	
		$3d$	$1d$	49·4	8·8 ± 1·5	0·023 ± 0·005	
D₂O	2·3	0 cm	8·4 cm	8·4	54·0 ± 1·2	0·231 ± 0·004	
		16·8 cm	8·4 cm	18·8	44·1 ± 1·2	0·188 ± 0·004	
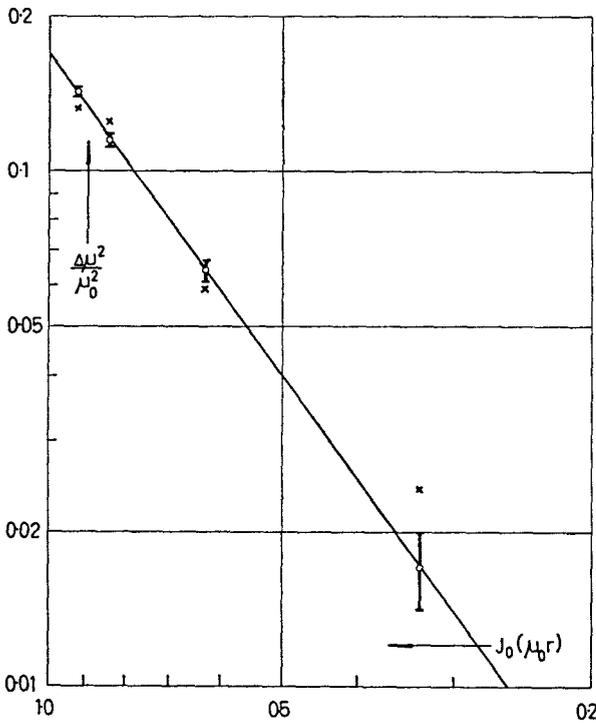
FIG. 13.—Radial buckling change $\Delta\mu^2/\mu_0^2$ caused by Cd-rods 2·3 cm dia. plotted against $J_0(\mu_0 r)$; lattice pitch $d = 16·8$ cm.

    × Exponential experiments;
    �I̷ Pulsed experiments;
    —— Const. $[J_0(\mu_0 r)]^n$.

FIG. 14.—Radial buckling change $\Delta\mu^2/\mu_0^2$ caused by Cd-rods 4·7 cm dia. plotted against $J_0(\mu_0 r)$; lattice pitch $d = 16·8$ cm.

    × exponential experiments;
    ⫯ pulsed experiments;
    —— const. $[J_0(\mu_0 r)]^n$.

where ν is the second root of equation (4.6), while S_ν, S_μ are the coupling constants given by equation (4.9); d_1 and d_2 are the extrapolation lengths of fast and thermal group neutrons. We assumed $d_1 = \infty$, while d_2 was taken from *Reactor Physics Constants* (ANL 5800) using $\lambda_t = 2·5$ cm as the transport mean free

path (Table 7). According to equation (6.7), $\Delta\mu^2/\mu_0^2$ depends on the ratio

$$-\frac{S_\nu}{S_\mu} = \frac{\tau}{L^2} \cdot \frac{k_\infty(1 - \beta)}{(1 + \tau B^2)^2} = -\sigma \qquad (6.8)$$

and therefore, in principle, on the buckling B^2. As is

seen from the results of equation (6.7) shown in Fig. 15 and from our experimental data as well, this dependence is not very much pronounced.

In order to check equation (6.7) within a somewhat larger buckling region, the effect of a 2·3 cm cadmium rod near centre ($x = 0, y = d$) was examined within two lattices ($d = 16·8$ and $18·0$ cm) employing the

TABLE 7.—THERMAL NEUTRON EXTRA-POLATION DISTANCE d_2 ON SURFACE OF Cd–ROD OF RADIUS ρ

ρ	d_2/λ_{tr}	d_2
1·15 cm	1·035	2·580 cm
2·35 cm	0·945	2·360 cm

Fourier analysis method described in Section 3.3. From the decay constants of the three lowest axial modes we obtain by means of Fig. 10 the corresponding radial buckling change $\Delta\mu^2/\mu_0^2$ which is plotted in Fig. 15 against the total buckling B^2 of the undisturbed flux mode in question. There is good agreement between experimental data and the theoretical curve derived from equations (6.7) and (6.6).
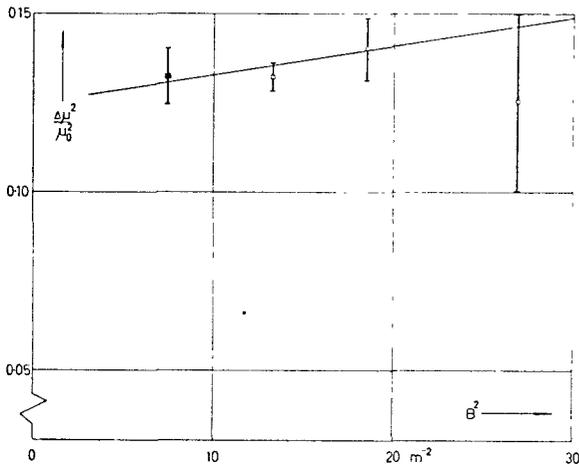

FIG. 15.—Radial buckling change $\Delta\mu^2/\mu_0^2$ due to a Cd-rod of 2·3 cm dia. as a function of geometrical buckling B^2; rod position near center ($x = 0$, $y = d$), lattice pitch $d = 16·8$ cm.

■ Exponential experiment ($B^2 = B_m^2$);

○ Pulsed experiments;

—— Calculated by two-group theory, equation (6.7).

For the lattice pitch $d = 16·8$ cm we measured, in addition, the reactivity effect of a cadmium rod placed at the position of one of the 4 central fuel elements. According to Table 6, the experimental value $\Delta\mu^2/\mu_0^2$ is found to be somewhat larger than the effect of a rod in the normal position increased by the effect of the missing fuel element which is given in the next section.

6.4 Reactivity contribution of single fuel rods

In a stationary exponential experiment we measured the change of the axial flux relaxation constant γ caused by the withdrawal of certain fuel rods. The lattice hole obtained by this may be considered as a local disturbance giving rise to a radial buckling change $\Delta\mu^2$ which is to be determined from the experimental value $\Delta\gamma^2$ as shown in Section 6.2.

Figures 16 and 17 present the experimental results obtained for a lattice pitch $d = 16·8$ and $13·2$ cm. In Fig. 16 we plotted $\Delta\mu^2/\mu_0^2$ against the number n of
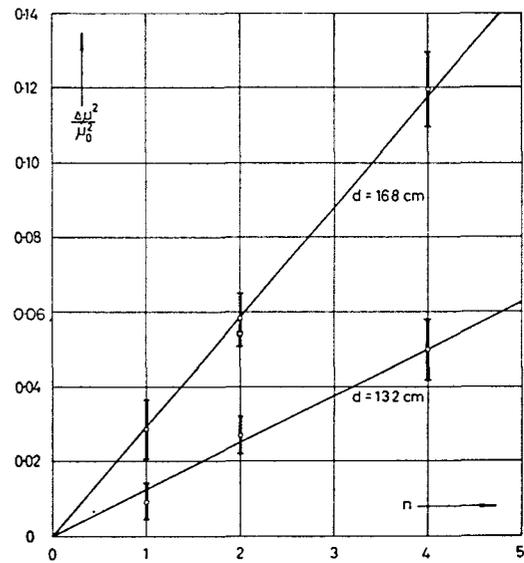

FIG. 16.—Radial buckling change $\Delta\mu^2/\mu_0^2$ as a function of number n of central fuel rods withdrawn from the lattice; exponential experiment ($d = 16·8$ and $13·2$ cm).

○ Neighbouring fuel rods;

□ Diametral fuel rods.

central fuel rods withdrawn from the assembly. In both cases, $\Delta\mu^2/\mu_0^2$ is proportional to n within the experimental error, indicating that there are no appreciable coupling effects between neighbouring fuel rods.

By the pulsed method we merely investigated the effect of the four central rods mutually withdrawn using the Fourier analysis technique (Section 3.3). From the experimental decay constants α_k of the three lowest modes we obtained $\Delta\mu^2/\mu_0^2$ by means of Fig. 10. Obviously, there is a large difference between results of stationary and pulsed experiments. As may be seen from a plot of $\Delta\mu^2/\mu_0^2$ vs. B^2 (Fig. 17) the reactivity effect markedly decreases with the geometrical buckling B^2 of the flux distribution. At $B^2 \approx 18$ m^{-2}, $\Delta\mu^2/\mu_0^2$ is zero and becomes even negative at still higher quantities of B^2.

The strong dependence on B^2 stated above may be explained by the boundary condition at the fuel element being extremely different for fast and thermal neutrons. The reactivity effect of a fuel element is composed of two contributions of opposite sign, that is to say, a positive fast neutron and a negative thermal neutron source effect. In the stationary case the
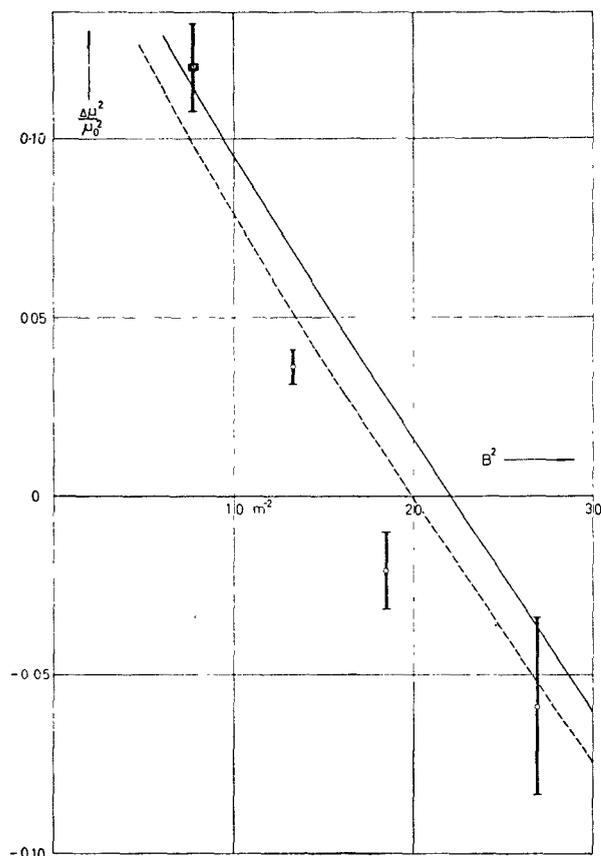

FIG. 17.—Radial buckling change $\Delta\mu^2/\mu_0^2$ caused by the withdrawal of 4 central fuel rods as a function of geometrical buckling B^2; lattice pitch $d = 16 \cdot 8$ cm.

$\dashv$ exponential experiment ($B^2 = B_m^2$);

$\ominus$ pulsed experiments;

— — — — Two-group perturbation theory, equation (6.10);

———— Two-group two-media solution.

positive effect predominates. At higher B^2, the importance function of the fast group decreases in favour of the thermal part according to the fast neutron leakage term $1/(1 + \tau B^2)$, leading to an increase of the negative thermal neutron source effect.

The moderator region arising from the withdrawal of n central fuel rods may be regarded as an inner reflector of effective radius $R_1 = \sqrt{n} \cdot d/\sqrt{\pi}$. According to two-group first-order perturbation theory

we have

$$\Delta\alpha = \frac{-\int_0^{R_1} \phi^2(r)r\, dr \frac{1}{l_2}\left(1 - \frac{k_\infty(1 - \beta)}{1 + \tau B^2}\right)}{\int_0^{R} \phi^2(r)r\, dr}$$

$$= -\frac{\pi R_1^2}{\pi R^2 J_1^2(\mu_0 R)}\frac{1}{L_2}\left(1 - \frac{k_\infty(1 - \beta)}{1 + \tau B^2}\right) \quad (6.9)$$

if the thermal neutron absorption in the reflector is neglected. By means of equation (6.3) we finally get the radial buckling change originating from the reflector zone

$$\frac{\Delta\mu^2}{\mu_0^2} = -\frac{1}{\mu_0^2 R^2 J_1^2(\mu_0 R)}\frac{R_1^2}{L^2}\frac{1}{1 - \sigma}\left(1 - \frac{k_\infty(1 - \beta)}{1 + \tau B^2}\right) \quad (6.10)$$

with σ given by equation (6.8).

The curves drawn in Fig. 17 were obtained from the perturbation formula equation (6.10) and from an exact two-group theory solution of the homogeneous two-media problem stated above. In both cases we have a pronounced decrease of $\Delta\mu^2/\mu_0^2$ with B^2, as for the experimental points. However, there are some deviations between experiments and homogeneous theory indicating that heterogeneous effects may be important.

REFERENCES

BENGSTON J. (1958) *Proceedings of the Second International Conference on the Peaceful Uses of Atomic Energy, Geneva,* P/1783. United Nations, New York.
CAMPBELL E. C. and STELSON P. H. (1956) ORNL-2204, p. 34.
EYRICH W. *Nukleonik* 4, 167 (1962).
FULTZ S. C. (1959) *Nucl. Sci. Engng.* 6, 313–319.
GLASSTONE S. and EDLUND M. C. (1957a) *The Elements of Nuclear Reactor Theory,* pp. 296, 238, 322. Van Nostrand Inc., New York.
HUGHES D. J. and SCHWARTZ R. B. (1958) *Neutron Cross Sections,* BNL-325.
KÜCHLE M. (1961) Karlsruhe Internal Report.
KUNZE H. (1962) To be published.
MEISTER H. (1961) *Nukleonik* 3, 236.
MEISTER (1962) To be published.
PERSSON R. *et al.* (1958) *Proceedings of the Second International Conference on the Peaceful Uses of Atomic Energy, Geneva,* P/160. United Nations, New York.
RADKOWSKY A. (1950) ANL-4476, p. 89.
Reactor Physics Constants (1958) ANL 5800 p. 169.
SILVER E. G. *et al.* (1960) *Trans. Amer. Nucl. Soc.* 3, (1) 278.
SIMMONS B. E. and KING J. S. (1958) *Nucl. Sci. Engng.* 3, 595.
SJÖSTRAND N. G. (1956) *Ark. Fys.* 11, 233.
WADE J. W. (1956) DP—163.
WEINBERG A. M. and WIGNER E. D. (1958) *The Physical Theory of Neutron Chain Reactors,* p. 485, Chicago University Press.